Sustainable Cities and Society 21 (2016) 51–65

Contents lists available at ScienceDirect

Sustainable Cities and Society

journal homepage: www.elsevier.com/locate/scs

An urban-forest control measure for ozone in the Sacramento, CA Federal Non-Attainment Area (SFNA)

Haider Taha[a,*], James Wilkinson[b], Robert Bornstein[c], Qingfu Xiao[d], Greg McPherson[e], Jim Simpson[e], Charles Anderson[f], Steven Lau[f], Janice Lam[f], Cindy Blain[g]

[a] Altostratus Inc., 940 Toulouse Way, Martinez, CA 94553, USA
[b] Alpine Geophysics (presently at Golder Associates), USA
[c] San Jose State University, USA
[d] University of California at Davis, USA
[e] U.S. Forest Service, Pacific Southwest Research Station, USA
[f] Sacramento Metropolitan Air Quality Management District, USA
[g] Sacramento Tree Foundation (presently at California Releaf), USA

ARTICLE INFO

Article history:
Received 6 September 2015
Received in revised form
13 November 2015
Accepted 18 November 2015
Available online 2 December 2015

Keywords:
Air quality
Air quality modeling
Biogenic emissions
Biogenic volatile organic compounds
Control measure
Meteorological modeling
Ozone
State implementation plan
Urban forest

ABSTRACT

Urban forest strategies of gradually replacing high emitters of biogenic volatile organic compounds (BVOC) with low-emitting species are being considered as voluntary or emerging control measures for maintenance of the 8-h ozone standard in the Sacramento Federal Non-Attainment Area (SFNA). We describe a regulatory modeling study demonstrating the air-quality impacts of such measures as well as of strategies that increase net canopy cover.

The results indicate that changing the mix of urban trees can improve air quality. The daily reductions in ozone resulting from species replacement alone reach up to 0.50 ppb. With a more geographically-targeted replacement, the daily reductions increase to 3 ppb. Population-weighted exposure to ozone is reduced by up to 34% relative to the NAAQS (120 ppb) and 12% relative to the CAAQS (90 ppb). The 8-h average peak ozone is reduced by 2%. If, in addition to species replacement, the net canopy cover is increased, the reductions in ozone become much larger but increases in ozone also occur. In some scenarios, the air-quality impacts are 10 times as large as those of only replacing 650,000 trees (control measure). Furthermore, because of the canopy growth (including the replacement trees) relative to 2000–2005, the SFNA is cooled by up to 1.2 °C by 2018 and 1.6 °C by 2023.

1. Introduction

Among several ozone air-quality improvement strategies, the Sacramento, CA region Air Districts are considering the use of urban forests to help the area maintain the 8-h standard. Under the current federal regulatory framework, an urban-forest strategy is considered a voluntary or emerging control measure. To include such a strategy in the area's State Implementation Plan (SIP), the air districts must quantify the benefits using best available science and technology, e.g., via meteorological, emissions, and photochemical modeling. This paper summarizes modeling performed to support the development of an urban-forest control measure for the SFNA. Two main scenarios and combinations thereof were examined:

(1) Replacement of 650,000 current-mix species (~3% of trees in the region) with lower emitters (control strategy).
(2) Net increase in canopy cover in newer *urbanizing* areas where forest cover will increase to match that in *urbanized* areas (auxiliary benefits).

The first scenario involves minimal impact on the region's meteorology or pollutant-deposition rates because no significant differences in vegetation cover, energy, and water balance of the replacement canopy are anticipated, nor changes in thermo-physical properties. In this case, only chemistry impacts resulting from reductions in emissions of biogenic volatile organic compounds (BVOC) can be expected. The second approach involves *both* meteorology and chemistry effects as well as changes in deposition rates.

Urban forests can impact air quality via several pathways, e.g., meteorological, deposition, emissions, and chemical. *Replacing* the

* Corresponding author. Tel.: +1 9252281573.
E-mail address: haider@altostratus.com (H. Taha).

http://dx.doi.org/10.1016/j.scs.2015.11.004
2210-6707/

current mix with low emitters (i.e., the control measure) is mostly a chemistry effect and results in decreased ozone concentrations. This is because the abundance of BVOC in the atmosphere allows ozone to accumulate via their reaction with nitric oxide (NO), reducing titration of ozone. Thus a control measure that can reduce VOC in the atmosphere, such as reducing BVOC from urban forests, can help reduce ozone accumulation.

However, *increasing* the canopy cover can impart both positive (beneficial) and negative (inadvertent) effects on air quality. Previous studies (e.g., Taha, 1996, 2005) have shown that the relative benefits and disbenefits differ from one region to another and that it is possible to maximize the potential benefits on a region-specific basis by locally optimizing the control strategies. These studies also showed that it is not possible to generalize the findings or extrapolate results from one area to another.

McPherson (1998) and Simpson and McPherson (2007) estimate that the regional urban forest in the Sacramento area consists of ~7 million trees from over 100 different species made up of 61% low emitters, 28% medium-emitting, and 11% high emitters. Through a combination of community education and policy change over a period of 10 years, the proposed control measure will cause 650,000 medium- and low-emitting trees to be planted that otherwise would have been higher emitters. This shift will reduce BVOC emissions by a quarter of a ton per day or more in the SFNA. In addition, the Sacramento Urban Forest Ecosystem Study (McPherson, 1998) concludes that the existing regional canopy in the Sacramento region is 14% in developed (urbanized) areas and 5% in undeveloped (urbanizing) areas slated for development. Thus another set of scenarios examined in this study includes increasing canopy cover in *urbanizing* areas from 5% to 14% to maintain the overall target cover in the region.

2. Models

2.1. Meteorological models

The MM5 mesoscale model and a variant of the fine-resolution UCP MM5 (uMM5) were used in this study. There were two reasons for this choice: (1) compatibility with regulatory modeling in California that was done with MM5 during 2005–2010, and (2) facilitate the coupling between the MM5 and the uMM5, a highly urbanized model, which would have been more difficult to achieve with other models. In this study, the uMM5[1] meso-urban meteorological model (Dupont, Otte, & Ching, 2004; Taha, 2008a,b,c) was used, along with the sub-mesoscale soil model (SM2-u) of Mestayer et al. (2004) to improve the characterization of urban heat islands, canopy-layer meteorology, vegetation canopy water and energy balance, and flow divergence/convergence in the urban canopy and boundary layers. The model, its application, and model-specific input are discussed in Dupont et al. (2004) and Taha (2007, 2008a,b,c).

It is to be noted that other models exist that are also dedicated to fine-scale urban modeling including the Town Energy Balance model (TEB) of Masson (2000) and several recent additions to the WRF model (Skamarock, Klemp, & Dudhia, 2008). These updates include the urban parameterizations of Martilli, Clappier, and Rotach (2002), which are also implemented in the uMM5, and those of Salamanca, Martilli, Tewari, and Chen (2011). The uMM5 is similar in features and capabilities to the urban WRF models but its configurations, data input development, and applications are different and more site-specific.

[1] The term "uMM5" is used here to refer to modifications and updates by Taha (2007, 2008a,b,c) to the UCP MM5 of Dupont et al. (2004) resulting in an updated version of the model.

The MM5 is described in detail in several papers and technical notes. For information, the reader is referred to Dudhia (1993), Grell, Dudhia, and Stauffer (1994), Seaman, Kain, and Deng (1996), Hong and Pan (1996), Hsie and Anthes (1984), Tao and Simpson (1993), Schultz (1995), Reisner, Rasmussen, and Bruintjes (1998), Anthes (1977), Kain and Fritsch (1993), Grell, Kuo, and Pasch (1991), Betts and Miller (1986), Pan and Mahrt (1987), Chen and Dudhia (2001), and Stauffer and Seaman (1990).

2.2. Emissions model

Biogenic emissions modeling was carried out with the SMOKE/BEIS3 models as discussed in Section 6.

2.3. Photochemical model

The CAMx photochemical model (Environ, 2003) was used after some modifications were made to input, dry deposition calculations, and other aspects as needed in this study to simulate the effects of urban forests in support the proposed control measure. CAMx and its required input are discussed in Yarwood, Morris, Yocke, Hogo, and Chico (1996) and Environ (2003).

3. Modeling episodes and domains

Two regulatory episodes used by the California Air Resources Board (ARB) and Air Districts were modeled. These are 27 July–4 August 2000, 5–14 July 1999, and future-year projections of the episodes (2018 and 2023). The horizontal meteorological modeling domains are shown in Fig. 1. Both episodes were modeled with 36, 12, and 4-km grids (the 36-km grids differ). This study also adds a fourth, 1-km grid (D04) for fine-resolution meteorological simulations with the uMM5 that are subsequently used to drive the fine-resolution (1-km) photochemical simulations. Model details, horizontal and vertical domain attributes, periods, and other information are discussed in Taha, Wilkinson, and Bornstein (2011).

The photochemical (CAMx) modeling domains were defined such that the 4-km grid was inscribed within the 4-km MM5 grid whereas the 1-km grid was inscribed within the uMM5 domain. The coarse (4 km) CAMx simulations were driven by the mesoscale MM5 fields whereas the fine (1 km) grid simulations were driven by the uMM5.

4. Surface characterization

This study applies different models at different scales and, thus, different parameterizations and corresponding surface characterizations are used in each domain. In the 36- and 12-km grids, surface characterization generally follows the standard procedure in the MM5 using pre-assigned properties except that some parameters were updated as discussed in Taha (2007) and Taha et al. (2011) mainly to reduce soil moisture in urban land use[2].

In the SFNA domain, a modified approach (Taha, 2005, 2007) is followed. This employs more recent and location-specific surface data, e.g., from updated land-based surveys, remote-sensing platforms, LiDAR, or aerial photography, and, in this case, more recent and more resolved land-use and land-cover (LU/LC) data (Xiao & Wu, 2008; Xiao, Wu, Simpson, & McPherson, 2009). Note that whereas the standard MM5 approach characterizes the surface physical properties based on LU information, this study's surface characterization is based on both LU and LC. Furthermore, both LU and LC characterizations in the SFNA were updated in this project.

[2] In general, urban soil moisture was over-estimated in some prior modeling efforts.

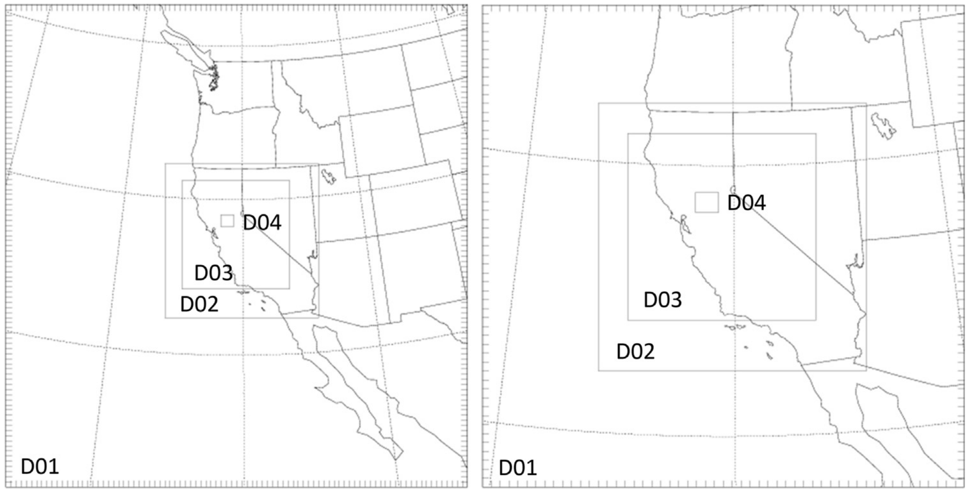

Fig. 1. Horizontal domain configurations for the July 1999 episode (left) and the July–August 2000 episode (right). Note that domains D02, D03, and D04 are similar in both episodes.

Surface characterization in this study is two-pronged. First, thermo-physical properties are assigned to LU classes which are then mapped to characterize the modeling domains. This part is termed "LU-based". In the second part, surface-specific values of thermo-physical properties are assigned to LC classes (this part is termed "LC-based"). The LC- and LU-based characterizations are then meshed.

The LU data is based on the 30-m USGS level-II classification system (Anderson, Hardy, Roach, & Witmer, 2001) as further improved upon and updated by Xiao et al. (2009) specifically for the SFNA. The LC data, on the other hand, is based on QuickBird/UFORE ("QBU4" for short) methodologies and analysis developed by McPherson (1998) and Xiao et al. (2009) to characterize land cover and vegetation in the Sacramento region. Because QBU4 data covers only parts of the meteorological/photochemical modeling domains and in many cases only parts of individual grid cells, a hybrid LU- and LC-based approach to surface characterization was followed in this study. The LC-based calculations apply to areas with QBU4 coverage whereas the LU-based characterizations apply to the remainder, non-QBU4 portion of each cell. Thus,

$$P = (1-u)P_{nu} + u\sum_i P_{ui}f_i \quad (1)$$

$$f_i = \frac{A_i}{A_u} \quad (2)$$

$$P_{nu} = \sum_j P_{nj}f_j \quad (3)$$

$$f_j = \frac{A_j}{A_{nu}} \quad (4)$$

where, P is the grid-cell value of a parameter to be computed, u is QBU4-data coverage in a grid cell, P_{nu} is the value of a parameter computed for the non-QBU4 portion of a grid cell, P_{ui} is the value of a parameter for a land *cover* "i" in the QBU4 portion of the grid cell, f_i is the fraction of land *cover* "i" in the QBU4 portion (thus is A_i/A_u)

Table 1
Parameters for LU-based calculations (summer). Z_o: cm, THC: cal cm^{-2} K^{-1} s$^{-0.5}$.

Land use		α	Z_o	η	THC
Urban					
11	Residential	0.157	85	0.10	0.03
12	Commercial/services	0.139	120	0.05	0.03
13	Industrial	0.152	120	0.05	0.03
14	Transportation/communication	0.117	35	0.02	0.03
15	Industrial and commercial	0.145	120	0.05	0.03
16	Mixed urban or built up	0.134	50	0.05	0.03
17	Other urban or built up	0.142	50	0.05	0.03
Agriculture					
21	Cropland and pasture	0.18	15	0.20	0.04
22	Orchards, groves, vineyards	0.16	20	0.20	0.04
23	Confined feeding operations	0.12	10	0.12	0.03
24	Other agricultural	0.15	10	0.18	0.03
Rangeland					
31	Herbaceous rangeland	0.18	12	0.15	0.04
32	Shrub and brush rangeland	0.18	20	0.15	0.03
33	Mixed rangeland	0.18	15	0.15	0.03
Forest					
41	Deciduous forest	0.13	70	0.30	0.04
42	Evergreen forest	0.13	70	0.30	0.04
43	Mixed forest	0.13	65	0.30	0.04
Water					
51	Streams and canals	0.08	2	1.0	0.06
52	Lakes	0.06	1	1.0	0.06
53	Reservoirs	0.08	1	1.0	0.06
54	Bays and estuaries	0.06	2	1.0	0.06
Wetland					
61	Forested wetlands	0.12	30	0.30	0.04
62	Non-forested wetlands	0.10	10	0.35	0.05
Barren land					
71	Dry salt flats	0.35	5	0.02	0.02
72	Beaches	0.35	5	0.06	0.03
73	Sandy areas (not beaches)	0.30	5	0.02	0.02
74	Bare rock	0.20	10	0.01	0.01
75	Strip mines and quarries	0.20	10	0.01	0.01
76	Transitional areas	0.18	6	0.02	0.02
77	Mixed barren land	0.18	7	0.02	0.02
Tundra					
81	Shrub and brush tundra	0.18	20	0.18	0.04
82	Herbaceous tundra	0.18	15	0.18	0.04
83	Bare ground	0.12	4	0.05	0.02
84	Wet tundra	0.10	7	0.35	0.04
85	Mixed tundra	0.10	7	0.20	0.04
Snow/Ice					
91	Perennial snowfields	0.70	2	0.95	0.05
92	Glaciers	0.35	5	0.90	0.05

Table 2
Parameters for LC-based calculations. Z_o: cm, THC: cal cm^{-2} K^{-1} s$^{-0.5}$.

Land cover	Z_o	α	η	THC	ε
Tree canopy	70	0.16	0.40	0.04	0.98
Shrubs	5	0.20	0.20	0.03	0.93
Grass	2	0.18	0.20	0.03	0.93
Bare soil	1	0.20	0.02	0.02	0.97
Roof	100	0.20	0.01	0.03	0.92
Paved	3	0.12	0.01	0.03	0.93
Water	0.01	0.06	1.0	0.06	0.99

where A_i is the area covered by land *cover* "i" and A_u is the total area of the QBU4 portion of a grid cell, P_{nj} is the value of a parameter for non-QBU4 portion and for land *use* type "j", f_j is fraction of land *use* type "j" in the non-QBU4 portion of a grid cell, thus is A_j/A_{nu}, where A_{nu} is the total area of non-QBU4 land-use in a grid cell.

Base LU-dependent input values to these calculations are summarized in Table 1 and the LC-dependent values in Table 2, where α is albedo, Z_0 is roughness length, η is soil moisture content, THC is thermal inertia, and ε is emissivity.

4.1. Note on albedo

Urban-forest scenarios evaluated in this study include: (1) species replacement and (2) increased canopy cover. In the first, we assume no changes in albedo as the replacement canopy is similar to the one being replaced. In the second scenario, albedo in each grid cell is recomputed based on the new distribution of vegetation cover (see also Section 8.1). In terms of photochemistry, those vegetation-related changes in albedo occur in the visible and near-infrared spectra (not in ultraviolet) and no impacts on photolysis rates are expected. Thus the chemistry effect of albedo modification from vegetation changes occurs via the temperature pathway alone.

4.2. Note on dry deposition

For dry-deposition calculations, the CAMx photochemical model uses an implementation of the Wesely (1989) algorithm which assigns roughness-length values (and thus deposition velocities) to each of 11 pre-defined LU categories. However, the pre-defined categories include only a single urban LU, which is not sufficiently resolved for detailed modeling. Thus in this study, roughness length was re-computed directly from gridded surface properties and used to override the input to CAMx.

5. Morphological input

Development of morphological parameters for this type of applications is discussed in Taha (2008a,b,c) and Taha et al. (2011). Here, a brief overview is provided.

5.1. Building canopy

Where site-specific morphometric data exist, e.g., Burian, Han, Velugubantla, and Maddula (2003), they were used directly in this study or further derived from Google Earth (Taha, 2008a,b,c). For those areas with urban LU and LC but no explicit morphology characterization, the gridded morphology parameters were developed based on representative vertical profiles of plan-, frontal-, and top-area densities (PAD, FAD, and TAD). For each grid cell, the building FAD and TAD can be computed if PAD information is available which, in this study, was derived from SFNA-specific building fractional cover as a function of the following LU classes (Xiao et al., 2009): (1) Residential (general), (2) Commercial and Services, (3) Industrial, (4) Transportation and Utility, (5) other urban/built-up, (6) Low density residential, (7) High density residential, (8) Multifamily residential, (9) Non-high-rise commercial, (10) High-rise commercial, (11) Urban high rise, and (12) Downtown core.

The building PAD profile is then computed for each 1-km grid cell for each vertical level (k) as:

$$\mathrm{PAD}_{1\,\mathrm{km}}(k) = \sum_{i=1}^{37} \mathrm{PAD}_i(k) f_i \tag{5}$$

where, PAD_i is the mean vertical profile for one of the LU categories identified above and f_i is the fraction of LU "i" in each 1-km grid cell. Note that the form of Eq. (5) is a result of using a vertical increment $\Delta z = 1$ m in this study.

5.2. Vegetation canopy

For vegetation canopy characterization, the process is similar to that for buildings. Vegetation mean vertical PAD profiles for 9 representative LU are defined as U.S. averages developed based on Burian et al. (2003) as shown in Fig. 2. Grid-level vegetation PAD is then computed with Eq. (5).

6. Biogenic emissions

BVOC emissions were calculated and merged with anthropogenic emissions for the regulatory episodes discussed in Section 3. The BVOC calculations use temperature and photosynthetically-active radiation (PAR) fields obtained directly from the meteorological models (MM5 and uMM5). In this study, emissions were updated for isoprene (ISOP), monoterpenes (TERP), methyl butenol (MBO), and other/oxygenated VOC (OVOC). Gridded emission rates (E) for a BVOC species were computed as:

$$E = E_1 f A + (1 - f) E_2 A \tag{6}$$

where A is the total area of a grid cell, f is fraction of the grid cell with QBU4 coverage, E_1 is QBU4 emission flux density, E_2 is non-QBU4 emission flux density (ARB emission rates).

6.1. ISOP and MBO emissions

These emissions were updated per Guenther, Zimmerman, Harley, Monson, and Fall (1993) as:

$$E = \xi E_s C_L^A C_T A \tag{7}$$

where, E is the total emissions rate from vegetated area A, ξ is a seasonal adjustment coefficient, E_s is the plant species-specific emissions flux at 30 °C and 1000 µmol m^{-2} s^{-1}, C_L^A is an environmental correction factor that accounts for changes in PAR as further attenuated by leaves (Eq. (10)), and C_T is a temperature correction factor that accounts for changes in leaf temperature. For ISOP, this correction factor is:

$$C_T = \frac{\exp\left[\frac{C_{T1}(T - T_S)}{R T_S T}\right]}{1 + \exp\left[\frac{C_{T2}(T - T_M)}{R T_S T}\right]} \tag{8}$$

where, C_{T1}, C_{T2}, and T_M are empirical coefficients, R is the ideal gas constant, T_S is an empirical normalizing temperature, and T is the leaf temperature, which is assumed to be the ambient temperature and taken from the meteorological model at the height specified in Table 3. For MBO, the correction factor (where T is again taken at the height specified in Table 3) is:

$$C_T = \frac{1.52\, C_{T2} \exp\left[\frac{C_{T1}(1/T_M - 1/T)}{R}\right]}{C_{T2} - C_{T1}\left\{1 + \exp\left[\frac{C_{T2}(1/T_M - 1/T)}{R}\right]\right\}} \tag{9}$$

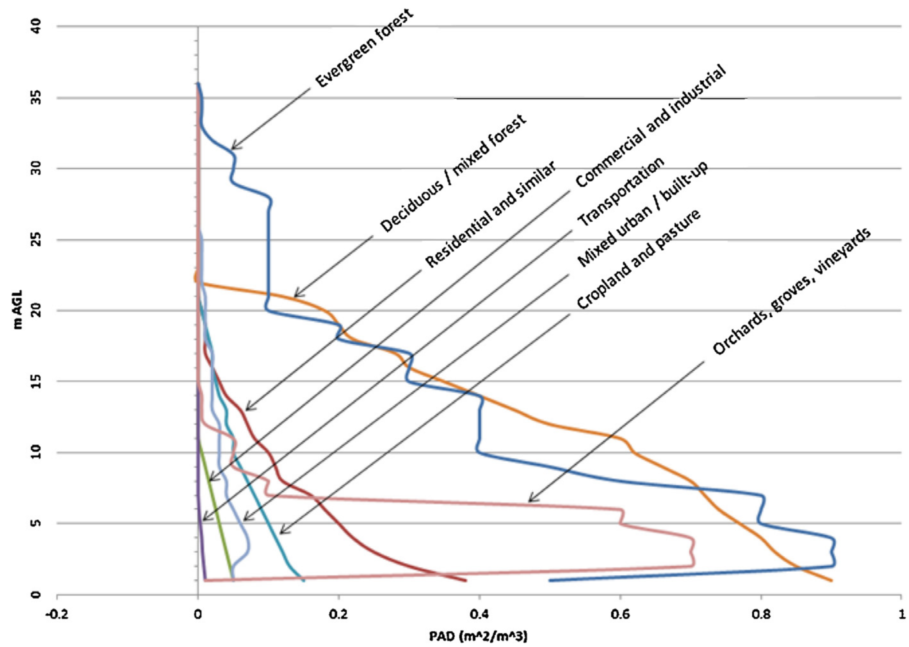

Fig. 2. Averaged vertical vegetation PAD profiles ($m^2\ m^{-3}$) for 9 land-use categories.

6.2. Temperature height

In this study, varying air–temperature heights (for T in Eqs. (8) and (9)) were used depending on each grid cell's LU/LC makeup. For each LU, a suitable temperature height was assigned as a function of vegetation-canopy PAD profiles shown earlier in Fig. 2. Table 3 summarizes the heights thus computed.

6.3. Canopy-adjusted PAR correction

The environmental correction factor for canopy-adjusted PAR in Eq. (7) was computed via a model that also accounts for the effects of variations over shaded and sunlit leaves (Campbell & Norman, 1998):

$$C_L^A = L_s^f C_L \,\mathrm{PAR_s} + L_D^f \, C_L \,\mathrm{PAR_D} \tag{10}$$

where, L_S^f is the fraction of sunlit leaves (Eq. (12)), L_D^f is the fraction of shaded leaves (Eq. (13)), C_L is the light correction factor (Eq. (11)), $\mathrm{PAR_D}$ is the diffuse fraction of $\mathrm{PAR_S}$ (on the shaded leaves), and $\mathrm{PAR_S}$ is the fraction of PAR on the sunlit leaves (direct + diffuse = 1). Here, PAR is taken from the meteorological model.

$$C_L = \frac{\alpha C_{L1} L}{\sqrt{1+\alpha^2 L^2}} \tag{11}$$

In Eq. (11), α and C_{L1} are empirical coefficients, and L is the PAR flux rate (taken from the meteorological model). Eqs. (12) and (13) define the fractions of sunlit and shaded leaves, respectively.

$$L_s^f = \frac{1-\exp(-k\,\mathrm{LAI})}{k\,\mathrm{LAI}} \tag{12}$$

$$L_d^f = 1 - L_s^f \tag{13}$$

where, κ is the direct beam solar radiation extinction coefficient (Campbell & Norman, 1998) and defined by Eq. (14) where θ is solar zenith angle (Duffie & Beckman, 1980), and LAI is derived from the PAD profiles shown in Fig. 2.

$$k = \frac{\sqrt{1+(\tan\theta)^2}}{2} \tag{14}$$

Table 3
Temperature-height assignments per LU/LC.

LU/LC description	USGS LULC mapping (crosswalk)	Temperature height (m AGL)
Residential	11	5.0
Commercial and services/industrial	12, 13, 15	7.5
Transportation/communications	14	2.0
Cropland and pasture	21, 24, 31, 32, 33, 81, 82, 84, 85	5.0
Deciduous/mixed forest	41, 43, 61	12.5
Bare land/water	23, 51, 52, 53, 54, 62, 71, 72, 73, 74, 75, 76, 77, 83, 91, 92	2.0
Mixed urban–built-up	16, 17	7.5
Orchards, groves, and vineyards	22	5.0
Evergreen forests	42	17.5

6.4. TERP and OVOC emissions

We estimate these emissions per Guenther et al. (1993) as:

$$E = \xi E_s C_T A \tag{15}$$

where, ξ is the seasonal adjustment factor, E_S is the plant species-specific emissions flux at 30 °C, A is the area occupied by the plant species, and C_T is the environmental temperature correction factor (Eq. (16)):

$$C_T = \exp\left[\beta(T - T_s)\right] \tag{16}$$

where, β is an empirical coefficient, T_S is the normalizing temperature scale, and T is ambient temperature at the heights given in Table 3.

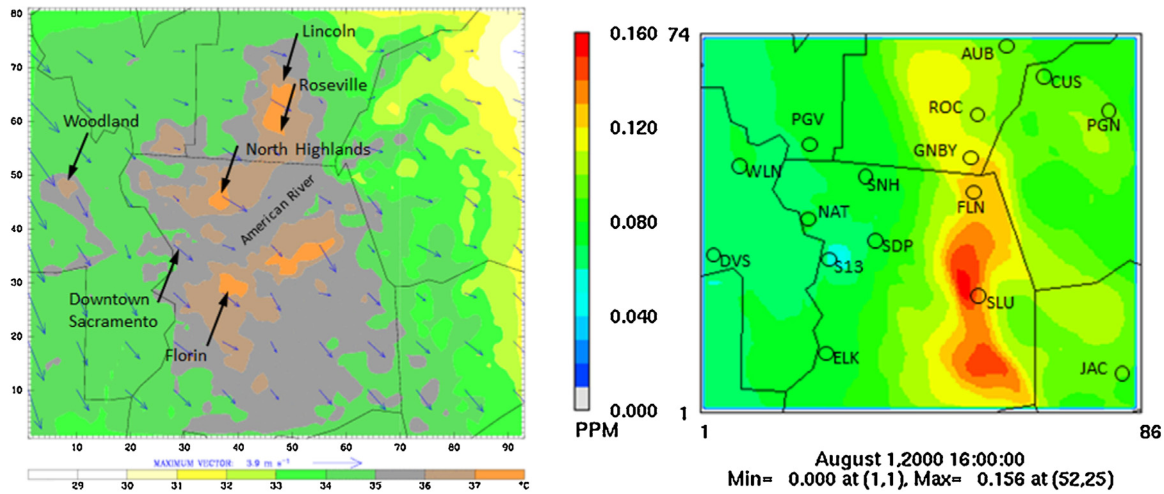

Fig. 3. a (left): Domain D04, 1-km model peak daytime heat island at 1500 PDT on 1 August (2000); 3b (right): 1-km model ozone at 1600 PDT on 1 August 2000. Selected monitors are also shown on this map (other monitors are shown in Fig. 8).

7. Reference case and model performance evaluation

7.1. Episode 27 July–4 August, 2000

Synoptic conditions during this episode were dominated by combined effects of the offshore Pacific high and a synoptic high over Arizona with day-to-day variations in their relative positions (i.e., extension of the Nevada high to eastern California) as discussed in detail in Taha et al. (2011). Upper-air flow was mostly southwesterly and southerly whereas the surface-level patterns were dominated by generally northwesterly flow in coastal areas with varying flow in eastern parts of the state. The modeled fields show coupling on some days, e.g., 30 July and 3 August, and some weak coupling on 28 and 29 July between the Sacramento area and the San Francisco region (which has implications on ozone and precursor transport). The modeled temperature highs in the Sacramento region range from the mid to high 30 °C throughout the episode, except on 1 August, where it reached 40 °C.

In terms of meso-urban fields, the model shows a daytime heat island of 2–3 °C (relative to time-varying upwind reference, non-urban temperature), except on 1 August where the UHI reaches the episode maximum of 4 °C. Areas around the American River are cooler than the rest of urban Sacramento by 1–2 °C (as seen in the cooler SW-NE corridor in Fig. 3a).

In terms of air quality, the model produces the observed fields, e.g., ozone concentrations and the downwind displacement relatively well. Taha et al. (2011) discuss the ozone simulations and various metrics in detail. The peak concentrations occur downwind of the Sacramento core because of chemistry time scales as well as advection of ozone and its precursors downwind. The modeled ozone in those locations depend on temperature, solar radiation, wind, and dynamics (PBL height, horizontal mixing). The modeled 1-km, 1-h peak is 109, 122, 134, 137, 121, 156, and 128 ppb, respectively on 27 July through 2 August. Fig. 3b is a sample of simulated ozone, in this case, the peak for 1 August (corresponding to Fig. 3a for meteorology).

7.2. Episode 5–14 July, 1999

At the beginning of this episode, the synoptic-scale pattern was marked by a high over Utah with southeasterly to southwesterly flow through much of California. On 8 July, the flow was mostly southerly in central parts of the state producing flow from SFBA to Sacramento. On 9 July, the flow was dominated by an offshore high as well as an inland high over Nevada producing northerly flow in southern California and southwesterly flow in central and northern California. During the last two days of the episode, the offshore high weakened and moved north thus changing the wind direction to northeasterly over much of central parts in the state.

In terms of mesoscale surface-level fields, the model shows daytime peak temperatures in the Sacramento area in the low 30's to 34 °C (the latter occurred on 8 and 9 July), 35 °C on 10 July, and 39 °C on 11 July. On 12 July (peak day), the model produces 41 °C in Sacramento, but only weak coupling with the San Francisco bay area. The region cools down on 13 July, so that the SFNA peak is only 34 °C. The model captures the observed tendencies well. In terms of daytime heat islands, the day-to-day variations range from 0.5 °C to 4 °C. The general spatial pattern of the heat island during this episode is similar to that of July–August 2000, and as demonstrated in general in Fig. 3a. The model shows strong coupling between San Francisco and Sacramento areas on 6, 9, and 10 July. Detailed discussion of the meteorology is provided in Taha et al. (2011).

In terms of air quality, the model produces the observed ozone concentrations relatively well. As with the 2000 episode, the peak concentrations occur downwind of the Sacramento core because of chemistry and advection scales. The modeled 1-km, 1-h ozone peak is 79, 117, 133, 145, 150, and 138, respectively on 7–12 July.

7.3. Model performance evaluation

Extensive model performance evaluation (MPE) was carried out (Taha et al., 2011) for both meteorological and photochemical models and that discussion will not be repeated here. In the following, a very brief summary of photochemical MPE is provided as an example. For MPE purposes, the ARB and Air Districts propose that the central California domain be divided into several zones as shown in Fig. 4. To be consistent, the same zones were used in this study. EPA-recommended photochemical-model performance benchmarks are (EPA, 1991, 1999): Unpaired accuracy of the peak (UA $\leq \pm 20\%$); Mean normalized bias (MNB $\leq \pm 15\%$); and Mean normalized gross error (MNGE $\leq 35\%$).

In Table 4, only MPE results for zone 6 (which includes the SFNA) are presented since it is the relevant area in this study. The monitors and observational data in this and other zones are discussed in Taha et al. (2011). Table 4 indicates that in the SFNA, all performance benchmarks are met or exceeded (compare the metrics with the benchmarks values in the last column).

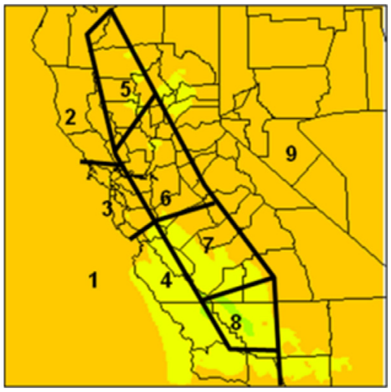

Fig. 4. Sub-domains for model performance evaluation–2: north coast; 3: San Francisco Bay Area; 4: south coast; 5: Central north; 6: Sacramento region; 7: SJV central; 8: SJV south; 9: inland.

Table 4
Zone 6 MPE indicators (%) for ozone.

Ozone metric (%)	7/28–8/2/2000	7/7–7/13/1999	Benchmarks
1-h MNB	−1.12	−13.22	≤ ± 15.00
8-h MNB	−0.04	−12.35	≤ ± 15.00
1-h MNGE	15.03	18.84	≤35.00
8-h MNGE	12.25	14.94	≤35.00
1-h UA	20.44	7.41	≤ ± 20.00
8-h UA	18.98	0.05	≤ ± 20.00

8. Results and evaluation of urban-forest scenarios

Several urban-forest scenarios were modeled and analyzed in this study, a subset of which (Table 5) is presented in this paper. The scenarios described in the table include (1) those involving mainly emissions control (rows 1–4), and (2) those involving emissions control and meteorology changes (row 5).

In scenarios with emissions control only, the replacement of species can be carried out in two manners: (1) uniformly, per deployment potential throughout the SFNA, and (2) geographically-optimized (targeted). Fig. 5a shows the spatial pattern of emissions reductions (e.g., isoprene in this case) in the 1-km domain for the uniform-distribution case (022-020 or 014-012). The distribution is based on LU and LC analysis of scenarios developed in this study. The colored grid cells show where the current-mix species are replaced with low emitters (LE). Furthermore, the red and green overlay contour lines show the areas where reductions in ROG emissions could have smaller (red) or larger (green) ozone-reduction impacts, respectively, based on atmospheric carrying capacity of precursors in the area (Taha, 2011; Taha et al., 2011).

In Fig. 5b, the same emission-reduction totals of Fig. 5a are (1) re-distributed in space (relocated towards the eastern parts of Sacramento and Placer counties, per contour lines depicted in Fig. 5a) and (2) refocused on smaller areas (instead of distributed over a larger number of grid cells as in Fig. 5a). This re-arrangement (scenarios 022c-020 or 014c-012) allows for larger ozone reductions from the same ROG emissions reduction totals (also see Section 8.3).

8.1. Meteorology

Strictly speaking, the control measure involves only species replacement. However, because of growth in existing urban-forest canopy (including the replacement trees) and because some scenarios also involve net increase in cover, the related effects of increased BVOC emissions and changes in meteorology are also analyzed. Based on analysis of Xiao et al. (2009), the total tree-canopy cover in the QBU4 area is 294 km^2 in years 2000–2005 that will grow to 351 km^2 in 2018, 378 km^2 in 2023, and 405 km^2 in the 2023_7M scenario (the latter includes an additional 2.5 M trees). This corresponds to an average tree cover of 17.9% in years 2000–2005, 20.6% in 2018, 21.9% in 2023, and 23.5% in 2023_7M scenario. Note that these numbers and percentages are relative to the QBU4 area, not entire SFNA domain in which case the vegetation fraction will be much smaller than listed above.

As tree cover increases, the areas of other land covers, e.g., roofs, pavements, soil, grass, etc., decrease reciprocally (this is an "above-the-canopy" view of land cover). Based on prior urban-fabric characterization studies of Sacramento and other areas (Akbari, Rose, & Taha, 1999; Rose, Akbari, & Taha, 2003) the following was found to be representative and thus used in this study: (a) that 40% of the increase in canopy cover is a decrease in soil area; (b) another 40% of the increase in canopy cover is a reduction in area of impervious ground surfaces; and (c) that 20% of the increase in canopy cover becomes a decrease in roof area.

The effects of canopy-cover changes on meteorology are seen mainly in surface and air temperature differences, with relatively smaller signals in the flow, mixing, and humidity fields. However, the photochemical modeling accounts for all meteorological effects including changes in vertical mixing, turbulent kinetic energy, boundary layer height, advection and transport, humidity, temperature, and radiation (Taha, 2008a,b,c). The impacts on air temperature consist overwhelmingly of cooling in the SFNA domain, e.g., Fig. 6. At the locations where canopy cover increases, the general impact on air temperature is a daytime reduction and a smaller or no effect at night. For the overwhelming number of days in both episodes, there are no significant changes in nocturnal air temperature. The decrease in temperature begins at sunrise and is detectable by 0800, peaks at 1400–1500, and vanishes at

Table 5
Urban-forest scenarios presented in this paper.

	Control strategy scenarios (differences)		Interpretation of the difference between the scenarios
	July–August 2000 episode	July 1999 episode	
1	022-020	014-012	Impacts of BVOC emission reductions from BAU to LE (650,000 trees replaced) in the 2018 timeframe. This is the control measure proper.
2	025-023	017-015	Impacts of BVOC emission reductions from BAU to LE in the 2023 timeframe (long-term effects of control measure).
3	027-026	019-018	Impacts of BVOC emission reductions from FM to LE in the 2023 timeframe (resulting from 4.5 million trees being switched from FM to LE).
4	022c-020	014c-012	Similar to 022-020 and 014-012 except that the spatial distribution of species replacements (from BAU to LE) is altered to maximize ozone reduction (Fig. 5b).
5	2023_7M	2023_7M	This is a scenario in 2023 where 4.5 M trees are converted to LE and an additional 2.5 M LE trees are planted in the SFNA.

Definitions: BAU: business as usual, current mix; LE: low emitters; FM: functional mix (smaller emissions than BAU, but higher than LE), low emitters: ≤1.0 $\mu g\,g^{-1}\,h^{-1}$, medium emitters: >1.0 and <10.0 $\mu g\,g^{-1}\,h^{-1}$, high emitters: ≥10.0 $\mu g\,g^{-1}\,h^{-1}$ (McPherson, 1998; Simpson & McPherson, 2007).

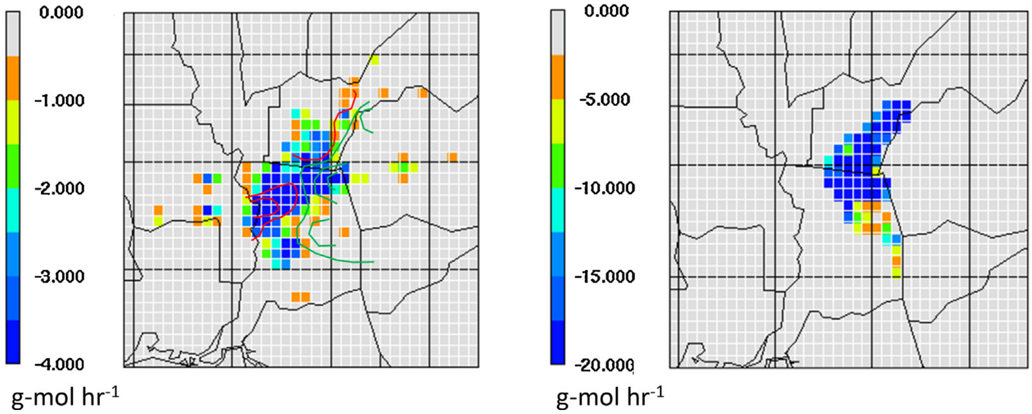

Fig. 5. a (left): Uniform distribution of isoprene emission reductions in the SFNA for 2018. The distribution is based on scenarios from QBU4 LU/LC analysis. Maximum decrease is 6.5 g-mol h^{-1} in any one grid cell (scale on the Figure is capped at 4 g-mol h^{-1} to show grid cells with small changes in emissions). Fig. 5b (right):The same emission reduction totals as in Fig. 5a are re-distributed (relocated towards the eastern parts of Sacramento and Placer counties) and refocused on smaller areas (instead of over a larger number of cells as in Fig. 5a). Maximum decrease is now 75 g-mol h^{-1} in any one grid cell (scale on the Figure is capped at 20 g-mol h^{-1} to show grid cells with smaller changes in emissions).

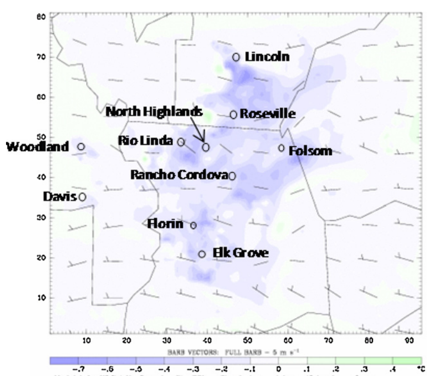

Fig. 6. Temperature difference (*C*) at 1500 PDT on 27 July for scenario 2018 (022-020) relative to present, caused by growth in canopy.

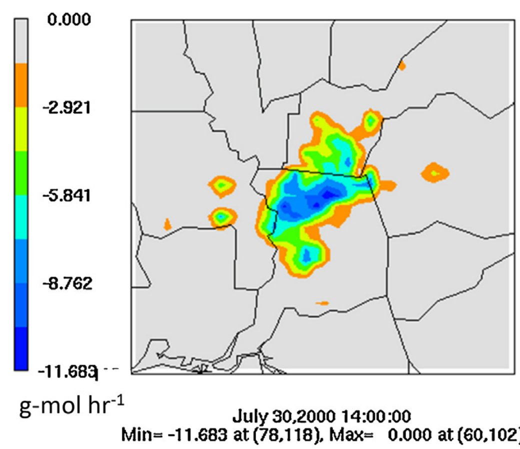

Fig. 7. Scenarios 025-023 isoprene emissions difference.

1900–2000 PDT. Table 6 summarizes impacts on air temperature for several scenarios in terms of the mean of daily largest temperature reductions. Some warming, up to 0.4–0.6 °C, occurs at times downwind of or around modified areas but the areas affected by warming are very small compared to those affected by cooling and thus not listed in Table 6. Fig. 6, for example, shows the extent affected by warming (small area highlighted in green, just west of Roseville) relative to the area affected by cooling (blue color over most of the region) at that hour.

In terms of boundary-layer (PBL) height, the simulations show that the nocturnal PBL is typically between 150 and 400 m at different locations in the SFNA. During the day, the PBL height peaks at 1.2–1.4 km between 1300 and 1800 PDT, and then starts decreasing again, repeating the diurnal cycle. The increase in canopy cover (scenarios involving meteorology) modifies various mechanisms that affect the PBL height, including transport of momentum, moisture, and heat. The growth of the tree canopy through 2018 causes no significant modifications to the boundary-layer depth throughout the day except for a few hours late in the afternoon where the PBL height changes by less than ±50 m (less than ±3.5%) in a few spots in the SFNA. The same pattern is seen for canopy growth through 2018, except that the PBL height changes in late afternoon (at a few spots) by less than ±10%. In the 2023_7M scenario, it changes by less than ±15% at a few locations in the SFNA. It is important to reiterate that the photochemical modeling in this study explicitly accounts for these changes in PBL depth among other meteorological variables.

Table 6
Mean of largest daily temperature reductions (95% confidence level).

	Mean of largest daytime cooling
July–August 2000 scenarios	
2018[a]	0.87 ± 0.10 °C
2023[a]	1.07 ± 0.10 °C
2023 7M[b]	1.20 ± 0.14 °C
July 1999 scenarios	
2018[a]	1.05 ± 0.09 °C
2023[a]	1.33 ± 0.13 °C
2023 7M[b]	1.50 ± 0.12 °C

[a] Growth in existing canopy (including replacement trees).
[b] Growth in existing canopy + additional new trees.

8.2. Emissions

Two aspects to BVOC-emission changes were evaluated. One is emission reductions from species replacement and the other a meteorology-related effect which, in turn, impacts emissions from both existing and new vegetation in the area. Fig. 7 is an example of spatial distribution of isoprene emissions reductions[3] for the hour

[3] Changes in emissions of monoterpenes, methylbutenol, and OVOC follow the same spatial pattern.

Table 7
BVOC emissions and changes for Sacramento county (mTPD) on two example dates.

Episode (example day)	case	ISOP	TERP	MBO	OVOC	Total BVOC (mTPD)
27 July 2000	020	10.10	7.16	4.22	8.51	29.99
	022	10.00	7.13	4.19	8.44	29.76
						$\Delta = -0.23$
	023	10.40	7.64	4.58	8.92	31.54
	025	10.20	7.59	4.50	8.80	31.09
						$\Delta = -0.45$
	026	10.00	7.47	4.50	8.70	30.67
	027	9.51	7.40	4.10	8.28	29.29
						$\Delta = -1.38$
7 July 1999	012	10.70	7.05	4.55	8.36	30.66
	014	10.60	7.02	4.51	8.30	30.43
						$\Delta = -0.23$
	015	11.00	7.53	4.94	8.75	32.22
	017	10.80	7.47	4.85	8.65	31.77
						$\Delta = -0.45$
	018	10.70	7.36	4.85	8.54	31.45
	019	10.10	7.29	4.42	8.13	29.94
						$\Delta = -1.38$

at 1400 PDT which is generally the time of largest changes. In this example, reductions correspond to scenarios 025-023 (see Table 5).

In the July–August 2000 episode, the difference between scenarios 022 and 020 (control strategy) translates into a maximum reduction of 7.24 g-mol h^{-1} of isoprene in any one grid cell. By comparison, cases 025-023 (Fig. 7) provide a maximum decrease of 11.68 g-mol h^{-1}, and scenarios 027-026 a maximum of 52.51 g-mol h^{-1}. In the July 1999 episode, the difference between scenarios 014 and 012 (control strategy) is a maximum reduction of 6.98 g-mol h^{-1} of isoprene in any one grid cell. In cases 017-015, the maximum decrease is 11.25 g-mol h^{-1} and in scenarios 019-018 it is 50.19 g-mol h^{-1}.

Table 7 provides a summary of BVOC emissions and changes in Sacramento County, for one example day in each episode. Because this is for Sacramento County only, the reductions in emissions are smaller (~60%) than the total reductions over the SFNA. While the control strategy (Simpson & McPherson, 2007) calls for a reduction of 0.27 mTPD of BVOC (isoprene, monoterpenes, and methylbutenol), the calculations in Table 7 also include OVOC emissions. The largest emission reductions occur in scenarios that involve meteorology changes. For the July–August 2000 episode, the largest changes are attained in scenarios 027-023 (−2.25 mTPD in Sacramento County) whereas for July 1999 episode they occur in scenarios 019-015 (−2.28 mTPD).

8.3. *Air-quality*

We quantify the impacts on ground-level ozone focusing on results from the 1-km grid shown in Fig. 1 (SFNA region). Changes in ozone are also evaluated at monitor locations in the area (monitors are described further in Taha et al. (2011) and shown in Fig. 8). In this section, the air quality impacts are discussed in terms of:

A. Largest daily changes in ozone (Section 8.3.1).
B. Cumulative changes at monitors (Section 8.3.2) to capture the overall effects (both positive and negative) during the length of the episodes.
C. Changes in RRF at monitors (Section 8.3.3) to capture the change in 8-h episodic maximum.
D. Population-weighted exceedance exposure (Section 8.3.4).
E. Changes in episodic 1-h maximum ozone at monitors (Section 8.3.5).

8.3.1. *Largest daily changes in ozone*

Table 8 summarizes the largest daily reductions in ozone for scenarios of emissions control only (no meteorology changes). Rows 1 and 2 represent the effects of control measure in 2018 and 2023, respectively. In row 3, differences are taken to diagnose the impacts of the strategy where 4.5 million FM trees are replaced with LE. This represents the relatively larger impact of the control measure (up to 1.52 and 2.93 ppb reductions). Note that since this difference is for going from FM to LE, the actual effects would have been larger if differences between BAU and LE were computed.

With geographically-optimized species redistribution (as in Fig. 5b), row 4 shows that larger benefits are achievable with the same total reductions in BVOC emissions as in scenarios 022-020 or 014-012, i.e., up to 0.75 versus 0.3 ppb in 2000 and 1.97 versus 0.47 ppb in the 1999 episode. A general observation can be made that in the 1999 episode, the ozone reductions overall are about 50% larger than in the 2000 episode and that the control measure is more effective under these conditions. This indicates that the urban-forest control measure can have significant and large beneficial effects depending on background emissions and meteorological conditions.

8.3.2. *Cumulative changes (CC)*

This metric simply is:

$$CC = \int_0^T \Delta(t)\,dt \tag{17}$$

where, $\Delta(t)$ is the difference between the perturbation and the reference unperturbed concentration, t is time, and T is the interval considered in the analysis[4].The CC metric (ppb-h) is applied to (1) daily peaks at each monitor and (2) all hours of the episode at each monitor. Analysis of differences for the peaks of the July–August 2000 episode (emissions-only control) indicates that the most effective scenarios are 025-023, 022c-020, and 027-026, the latter being the largest. Scenario 022c (converting BAU to LE with spatially-optimized replacements) can be up to 3 or 4 times more effective than the control strategy with uniformly-distributed species replacements. The results also indicate that the effects in

[4] In this discussion, the county codes are 067 for Sacramento, 113 for Yolo, 017 for El Dorado, and 061 for Placer.

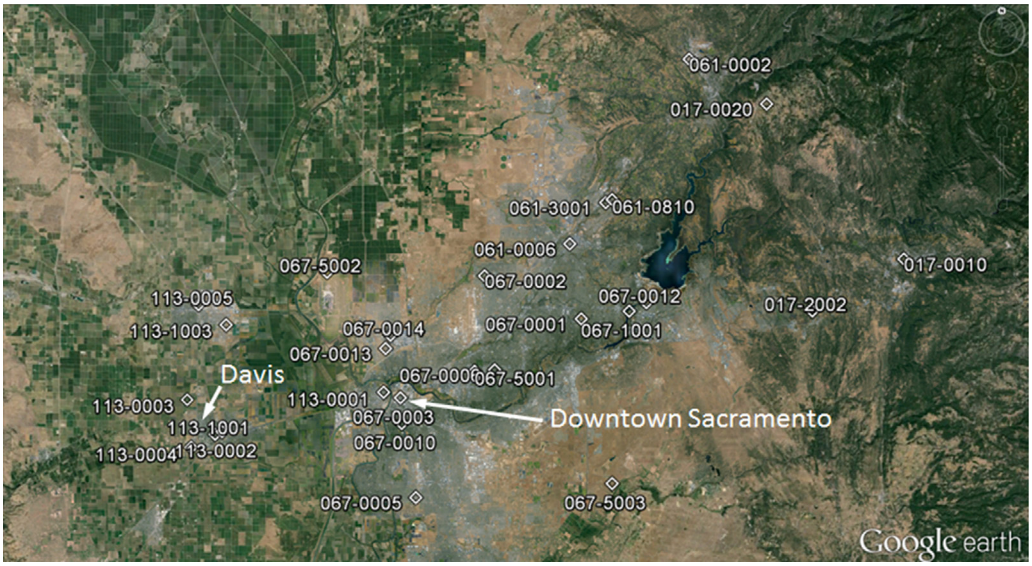

Fig. 8. Locations of air-quality monitors presented in the following discussion and figures. Monitor 067-0011 is not shown as it is further outlying to the south of this area.

2023 are about 50% larger than in 2018, thus continued long-term benefits from the control strategy.

In Fig. 9, total ppb-h changes are shown for all hours (not only peaks) for the scenarios of emission control only (no meteorology control). The most effective scenarios are 025-023, 022c-020, and 027-026, where the latter has the largest effect.

For scenarios of increased canopy cover, effects include increased emissions from the new canopy, decreased emissions from the existing canopy due to cooling, and other impacts on meteorology (as discussed in Section 8.1), thus on photochemical production of ozone. Among these scenarios, the largest to smallest impacts are 027-023, 027-025, and 026-023, and there are both increases and decreases in peak ozone. The results in Fig. 10 show that the impacts on all-hours ozone are predominantly a decrease with instances of increase (occurring at downwind sites). The results suggest that the effect of meteorology (benefits of cooling) is somewhat more pronounced on non-peak ozone than on peaks.

The increases in ozone occur mostly at some of the downwind monitors such as Sloughouse (067-5003), Auburn (061-0002), Ponderosa (017-2002), and Roseville (061-0006). However, as discussed above, if the additional canopy is concentrated relatively more in the eastern part of the domain, the effects will be larger and more dominant decreases in ozone. Finally, comparing scenarios 027-023 and 026-023 shows that using LE species in the 2023_7M scenario rather than FM species is significantly more effective (up to 2–3 times larger). There are also monitors where the FM scenario does not produce any reduction in ppb-h while the LE scenario produces such reductions. Finally, at those locations where there are increases in ozone, the LE scenario produces smaller increases than the FM scenario.

For the July 1999 episode, the ppb-h differences of the peaks at monitors for the emissions-control scenarios are larger than in the July–August 2000 episode. They are about twice as large and sometimes more because of different meteorology and emissions. The most effective scenarios are 017-015, 014c-012, and 019-018, the latter being the best. This is the same order of scenario effectiveness as in the July–August 2000 episode. Converting BAU to LE with spatially optimized species replacements can be up to 3 or 4 times more effective than the control strategy with uniformly-distributed replacements. Furthermore, the effects of converting BAU to LE in 2023 are about 50–100% larger than in 2018 (thus sustained long-term benefits) and the effects in future years of the 1999 episode are larger than the future-year effects in the July–August 2000 episode.

In Fig. 11, total ppb-h changes are shown for all hours for the emission-control scenarios. Compared to the July–August 2000 episode (Fig. 9), the effects in the July 1999 episode are roughly twice as large. The most effective scenarios are those 017-015, 014c-012, and 019-018, the latter being the best.For scenarios with meteorology changes, the order of effectiveness (from largest to smallest impacts) is 019-015, 019-017, and 018-015. There are both increases and decreases in peak ozone because of increases in emissions but also cooling effects. However, the reductions in these scenarios are more dominant than the increases, indicating an overall effectiveness of meteorological changes (cooling) in compensating for and partially offsetting the effects of increased BVOC emissions. Except for scenario 018-015, the other two scenarios produce only minor increases in ozone but overwhelmingly a decrease (Fig. 12). The results in Fig. 12 show that the impacts on all-hours ozone are overwhelmingly a decrease with the exception of one monitor at Elk Grove (067-0011) and one in Woodland (113-1003). Overall, the urban-forest scenarios produce more (and

Table 8
Largest reductions in ozone for species replacement only (no meteorology changes).

	Basis: July–August 2000			Basis: July 1999		
	Scenarios	Largest daily O3 reduction (ppb)	Mean of largest daily reduction (ppb)[a]	Scenarios	Largest daily O3 reduction (ppb)	Mean of largest daily reduction (ppb)[a]
1	022-020	0.30	0.16 ± 0.014	014-012	0.47	0.21 ± 0.028
2	025-023	0.37	0.25 ± 0.015	017-015	0.74	0.36 ± 0.049
3	027-026	1.52	1.01 ± 0.053	019-018	2.93	1.40 ± 0.190
4	022c-020	0.75	0.56 ± 0.028	014c-012	1.97	0.90 ± 0.120

[a] 95% confidence level.

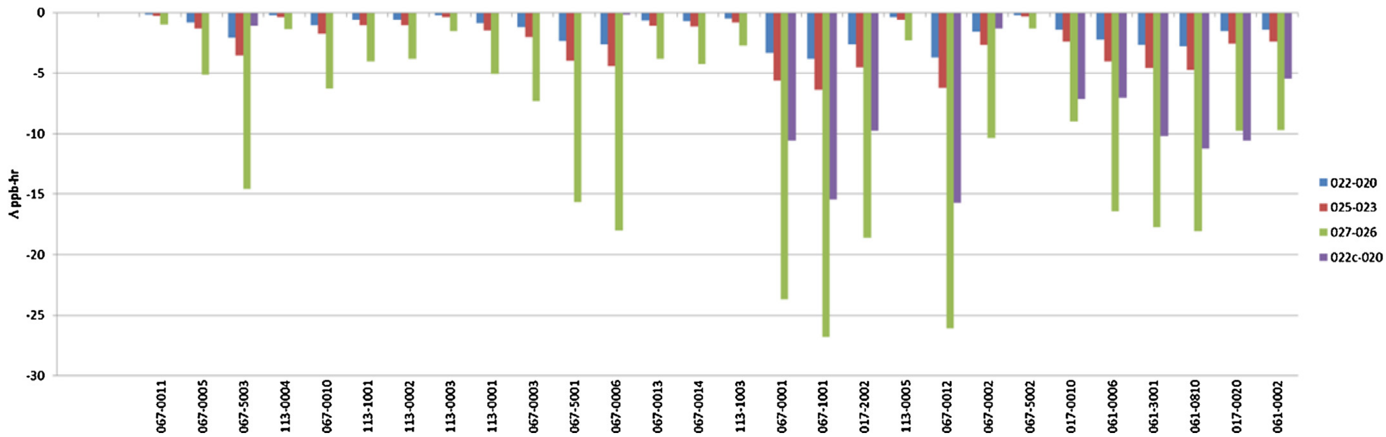

Fig. 9. ppb-h difference for all hours (2000 episode).

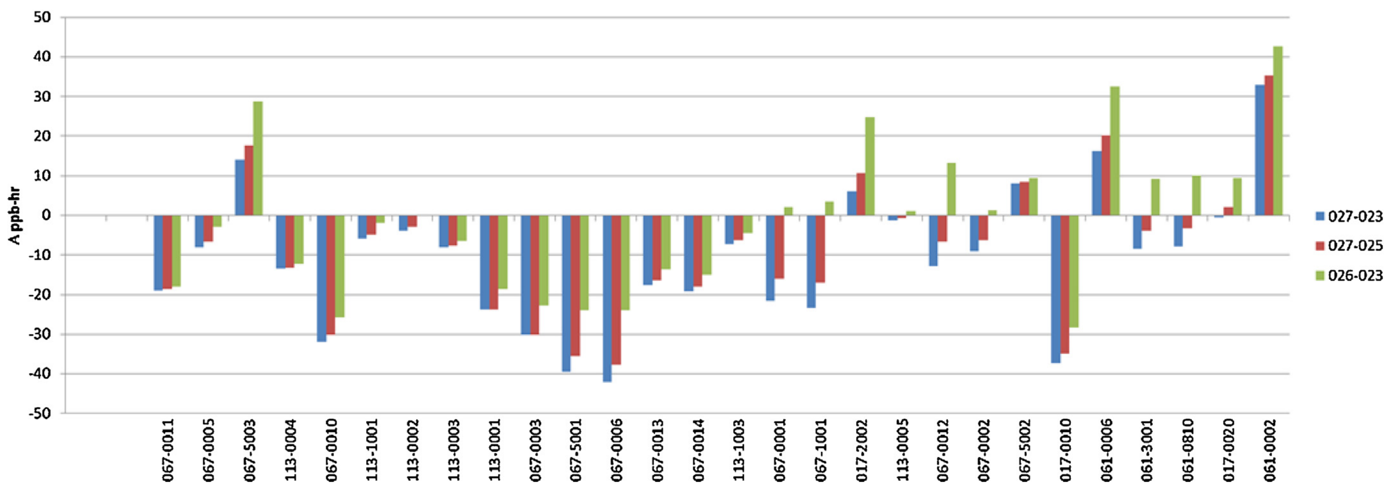

Fig. 10. ppb-h difference for all hours (future year scenarios of the 2000 episode) for cases involving increased canopy cover.

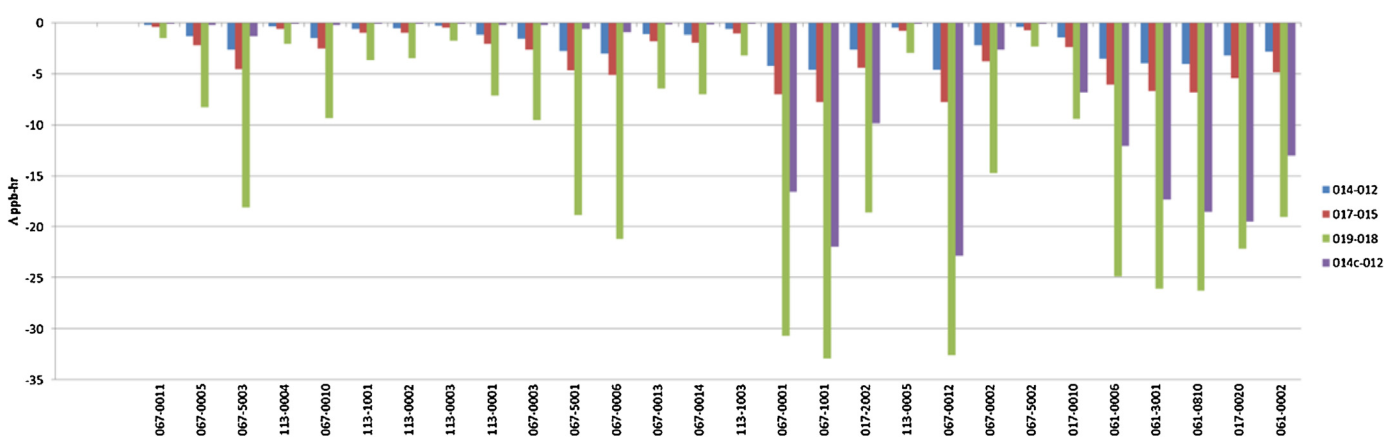

Fig. 11. ppb-h difference for all hours (future year scenarios of the 1999 episode).

larger) reductions and less (and smaller) increases in ozone during the July 1999 episode compared to the July-August 2000 episode (e.g., compare Fig. 12 with Fig. 10).

Comparing scenarios 019-015 and 018-019 shows, as with the 2000 episode, that the use of LE species in the 2023_7M scenario rather than FM is significantly better at improving air quality (up to 2–3 times larger). In addition, at those locations where there are increases in ozone, the LE scenario produces smaller increases than FM and, sometimes, the LE scenario produces decreases in ozone.

8.3.3. *Episodic 8-h maximum and RRF*

The 8-h peaks and relative reduction factors (RRF) were computed for each episode, monitor location, and scenario. For the July–August 2000 scenarios of emission control only, the changes in 8-h episodic maximum reach up to −0.07% for 022-020, −0.12% for 025-023, −0.50% for 027-026, and −0.18% for 022c-020. Thus the most effective scenario is the replacement of FM trees in 2023_7M with LE species. Also, the effect of concentrating the replacement trees in the eastern part of the domain is about twice as large as the

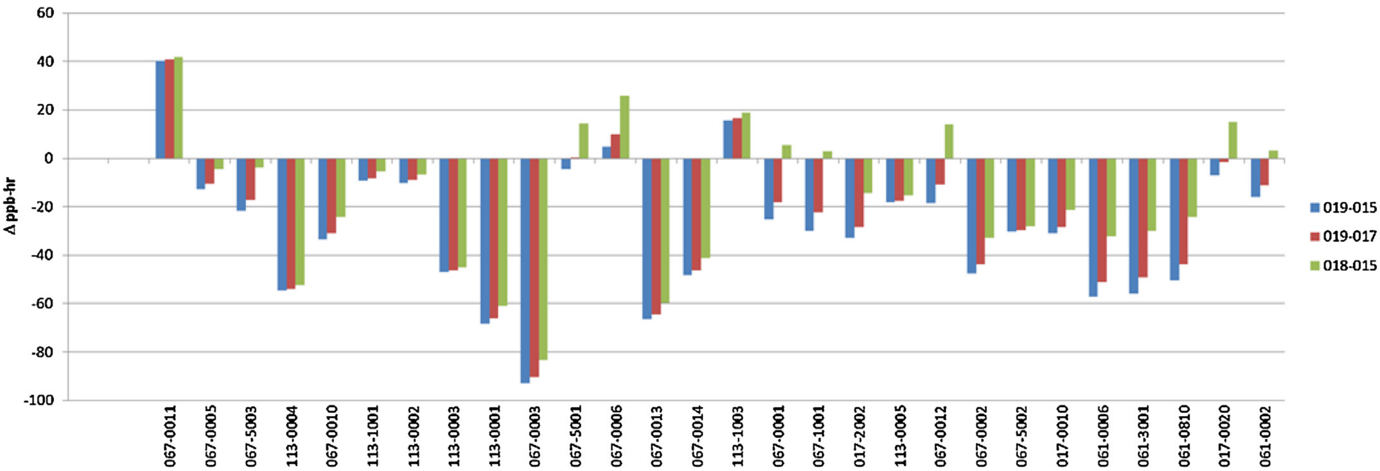

Fig. 12. ppb-h difference for all hours (future year scenarios of the 1999 episode) for cases involving increased canopy cover.

effect of the control measure with uniformly distributed replacements (for the same total BVOC emissions reductions).For scenarios that include net cover increase, emission changes, and meteorology impacts, e.g., scenarios 027-023, 027-025, and 026-023, many locations see a reduction in 8-h episodic maximum, but some see an increase, particularly downwind. Re-distributing the replacement trees in the eastern part of the domain can prevent or minimize these increases in ozone. Furthermore, the reductions in 8-h maximum in scenario 2023_7M using LE species (026) are up to 5 times larger than when using FM trees (026) and in cases where scenario FM increases the 8-h maximum, scenario LE either decreases it or does not increase it significantly.For the July 1999 scenarios of emission control only the effects (RRF) are about twice as large relative to the July–August 2000 episode. The changes reach up to −0.14% for 014-012, −0.24% for 017-015, −1.02% for 019-018, and −0.67% for 014c-012. Again, the effects of geographically-optimizing the replacement trees in the eastern part of the domain are about 2–4 times as large as the effect of the control measure with uniformly distributed replacement species.

For scenarios involving cover increase, emission changes, and meteorology, e.g., cases 019-015, 019-017, and 018-015 during the July 1999 episode, the impacts are overwhelmingly a reduction in the 8-h maximum, except for a small number of increases (resulting mainly from scenario 018). Unlike in the July–August 2000 episode, the net canopy-cover increase produces very beneficial and larger effects in the July 1999 episode. The results also show that reductions in 8-hr maximum in scenario 2023_7M using LE species (019) are up to 2–3 times larger than when using FM (018). In cases where the FM scenario increases the 8-h maximum, scenario LE actually decreases it. While scenario 018 can cause some increase in ozone, scenario 019 does not (except for one instance). This suggests that for scenario 2023_7M, the implementation should be carried out using LE tree species.

8.3.4. *Population-weighted exceedance exposure*

Exceedance exposure (E) is:

$$E = \sum_{x=1}^{X}\sum_{h=1}^{H} P_{(x)} \left\{ C_{i,x,h} - C_t \right\} H_{(\Delta c)} \tag{18}$$

where, x,X are spatial dimensions, h,H are temporal (hourly) dimensions, $P_{(x)}$ is population at location x, $C_{i,x,h}$ is ozone concentrations for scenario i at location x and time h, C_t is the concentration threshold, e.g., 120 (NAAQS) or 90 ppb (CAAQS), and H is defined as:

$$H = \begin{cases} 1 & (C_{i,x,h} > C_t) \\ 0 & (C_{i,x,h} \le C_t) \end{cases} \tag{19}$$

Table 9 summarizes changes in exposure in the SFNA region. For the July–August 2000 episode (rows 1–7), the control strategy can, at the minimum, reduce population-weighted exceedance exposure by between 1.13% and 3.52% with respect to 120 ppb and between 0.33% and 1.71% relative to 90 ppb (occurring on different days). These are relatively significant reductions considering the very limited credit allowed for the control measure. If additional effects are allowed, as the rest of the table shows, decreases in population-weighted exceedances can be large, in some cases providing a complete offset.

Among the scenarios involving only species replacement (rows 1–4), scenario 027-026 has the largest impacts on reducing population-weighted exceedance exposure, between 6.79% and 31.36% above 120 ppb and between 2.20% and 11.74% with respect to 90 ppb. For the scenarios involving canopy-cover increase, emissions changes, and meteorology (rows 5–7), the largest reductions in population exposure are attained with scenarios 027-023, up to 71.33% relative to 120 ppb and up to 99.08% relative to 90 ppb. It is also evident that for the 2023_7M scenario, the use of LE species (027-023) produces larger reductions in exposure than the use of FM species (026-023) and that the latter causes significant increases in exposure.

For the July 1999 episode (rows 8–14), the control strategy (014-012) can reduce population-weighted exceedance exposure in the SFNA by between 1.25% and 6.03% with respect to 120 ppb and between 0.35% and 1.02% relative to 90 ppb. The scenario with geographically-optimized planting (014c-012) produces 2–3 times the reductions in population-weighted exceedance relative to 014-012. For scenarios involving canopy-cover increase, emissions changes, and meteorology (rows 12–14), some of the larger reductions in population exposure are attained with scenarios 019-015, up to 37.88% relative to 120 ppb and up to 9.12% relative to 90 ppb. Note that 018-015 can cause significant increases on certain days.

8.3.5. *Change in episodic 1-h peak*

Simulations of the July–August 2000 episode show that the largest changes for the replacement scenarios are: −0.12 ppb for 022-020, −0.19 ppb for 025-023, −0.83 ppb for 027-026, and −0.23 ppb for 022c-02. For scenarios involving changes in

Table 9
Changes in population-weighted exceedance exposure (relative to given thresholds) for future-year scenarios of the July–August 2000 base episode (rows 1–7) and July 1999 episode (rows 8–14). NE: No exceedance above given threshold.

Year 2000		Threshold (ppb)	27-Jul (%)	28-Jul (%)	29-Jul (%)	30-Jul (%)	31-Jul (%)	1-Aug (%)	2-Aug (%)
1	022-020	120	NE	NE	−1.89	−1.13	NE	−1.27	−3.52
		90	−1.71	−0.63	−0.33	−0.35	−0.95	−0.34	−0.78
2	025-023	120	NE	NE	−2.92	−1.74%	NE	−2.06	−4.48
		90	−2.70	−1.07	−0.54	−0.58	−99.05	−0.56	−1.30
3	027-026	120	NE	NE	−12.26	−6.79%	NE	−8.35	−31.36
		90	−11.74	−4.15	−2.20	−2.36%	−5.74	−2.30	−5.47
4	022c-020	120	NE	NE	−3.92	−2.49	NE	−1.70	−5.34
		90	−7.13	−1.28	−0.58	−0.58	−3.78	−0.57	−0.86
5	027-025	120	NE	NE	−9.76	−2.13	NE	−4.97	−69.98
		90	−9.99	0.92	0.67	−0.76	−2.90	−0.93	−10.92
6	027-023	120	NE	NE	−12.39	−3.83	NE	−6.93	−71.33
		90	−12.42	−0.16	0.13	−1.34	−99.08	−1.48	−12.08
7	026-023	120	NE	NE	−0.15	3.18	NE	1.55	−58.23
		90	−0.77	4.16	2.38	1.05	−99.02	0.84	−7.00

Year 1999		Threshold (ppb)	7–Jul	8–Jul (%)	9–Jul (%)	10–Jul (%)	11–Jul (%)	12–Jul (%)
8	014-012	120	NE	NE	−6.03	−1.82	−1.25	−1.44
		90	NE	−0.92	−1.02	−0.59	−0.88	−0.35
9	017-015	120	NE	NE	−8.49	−3.07	−2.31	−2.58
		90	NE	−1.58	−1.66	−0.98	−1.46	−0.60
10	019-018	120	NE	NE	−33.90	−13.62	−11.53	−9.46
		90	NE	−6.56	−6.84	−4.25	−5.56	−2.28
11	014c-012	120	NE	NE	−20.92	−4.56	−0.63	−2.99
		90	NE	−5.13	−2.70	−1.00	−1.93	−0.62
12	019-017	120	NE	NE	−32.11	−16.31	4.81	3.44
		90	NE	−7.66	−7.66	−4.58	6.25	−2.60
13	019-015	120	NE	NE	−37.88	−18.88	2.39	0.77
		90	NE	−9.12	−9.20	−5.51	4.70	−3.18
14	018-015	120	NE	NE	−6.01	−6.09	15.74	11.31
		90	NE	−2.74	−2.54	−1.31	10.86	−0.92

emissions and meteorology, there are both increases and decreases in the peaks. On the average (domain-wide), the change in the 1-h peak is −0.1, −0.03, and 0.21 ppb for cases 027-023, 027-025, and 026-023, respectively. These are relatively small changes compared to those in non-peak metrics discussed earlier.

For the July 1999 episode, the largest changes for the emissions-control scenarios are: −0.21 ppb for 014-012, −0.36 ppb for 017-015, −1.31 ppb for 019-018, and −0.89 ppb for 014c-012. For scenarios with cover increase, emissions changes, and meteorology variations, the sum (cumulative) changes in the 1-h peaks are −35.92 ppb for scenarios 019-015, −33.33 for 019-017, and −25.00 for 018-015. Two observations can be made: (1) that the reductions of the 1-h peaks in the July 1999 episode are much larger than in the July–August 2000 episode, and (2) that the implementation of the 2023_7M scenario with LE species produces larger decreases in the 1-h peaks (about 50% larger) than using FM species. On the average (domain-wide), the change in the 1-h peak is −1.3, −1.2, and −0.9 ppb for the three cases, respectively, which are significant, much more so that in the 2000 episode.

9. Conclusions

This study evaluated the potential meteorological, emissions, and ozone air-quality impacts of an urban-forest control measure in the Sacramento Federal Non-Attainment Area (SFNA). The control measure includes replacing current-mix species with medium and low emitters of biogenic volatile organic compounds (BVOC) and, in the future, increasing the net canopy cover. The modeling indicates that changing the mix of urban trees can improve ozone air quality modestly to moderately and that if the changes in the mix are also accompanied by a net increase in canopy cover, the reductions in ozone become much larger. However, in the latter case, there can also be significant increases in ozone.

Considering both regulatory episodes modeled in this study, the largest daily reduction in air temperature (due to growth of canopy, including replacement trees) is 0.7–1.2 °C in 2018, 0.9–1.6 °C in 2023, and 1.0–1.8 °C in 2023, the latter including an additional 2.5 M new trees planted. Such changes in air temperature are significant and have large impacts on local meteorology, emissions, and air-quality. However, the control measure allows credit only for emission reductions and the rest is considered auxiliary benefits.

The results show a range of impacts on ozone depending on the scenario and level of canopy modifications. In terms of largest daily reductions, the most effective scenario produces a reduction of up to 1.5 ppb (in 2000 episode) and 3 ppb (in 1999 episode). For both episodes, this is a scenario in which the current, functional mix (FM) of species is replaced with medium and low emitters (LE). The effect of spatially redistributing species replacement in the SFNA (geographically-optimized) is to double or quadruple the effects of the control measure on ozone, with reductions of 0.75 and 1.97 ppb up from 0.30 and 0.47 ppb, respectively.

While replacement-only scenarios consistently produce reductions in ozone (in varying degrees depending on modifications), scenarios with increase in canopy cover can produce larger decreases in ozone (up to 10 times larger) but also increases. Thus it is important to select an optimal combination of control strategies that will locally maximize the benefits and minimize the inadvertent, negative impacts on air quality.

In terms of cumulative metrics (ppb-h) over monitors in the SFNA, the effects of all scenarios are larger in the July 1999 episode than in July–August 2000, about 50% larger for cases with species replacements only and 3–4 times larger in cases with cover increase and meteorology changes. The effects of the control strategy in the 2023 timeframe is 60–70% larger (or more) than in the 2018 timeframe thus indicating continued and significant long-term benefits from this control measure. The most effective scenario in impacting the peak ozone in the SFNA is that of switching 4.5 M trees from FM to LE, whereas the most effective scenario impacting all-hours ozone is that of adding 2.5 M LE trees to the urbanizing areas in the SFNA and converting 4.5 M existing BAU trees to LE. Averaged over the two episodes, the effect of this scenario is 10 times that of changing 650,000 trees from BAU to LE.

In terms of population-weighted exceedance exposure to ozone, scenarios involving only emissions control, i.e., species replacement only, result in reductions of up to 31.36% relative to 120-ppb and 11.74% relative to the 90-ppb threshold (for the 2000 episode). For the 1999 episode, the reductions are 33.90% relative to 120 ppb and up to 8.23% relative to 90 ppb. In cases involving canopy-cover increase, the changes are larger.In concluding, the study shows that the air-quality effects of the proposed urban-forest control measure are beneficial. However, if canopy cover is increased, the relative levels of benefits and negative effects depend on meteorological, emissions, and land-cover conditions in each area and scenario. Further research is needed to evaluate this strategy in more detail and its effects on the long term. The methods developed in this study can be applied elsewhere to evaluate the potential benefits of urban-forest measures in other areas and different climates.

Acknowledgements and Disclaimers

This paper summarizes work sponsored by the Sacramento Metropolitan Air Quality Management District (SMAQMD) under Contract E2007008 “Urban Forest for Clean Air Demonstration Project” (UFFCA) with Altostratus Inc. Findings in this paper do not necessarily reflect the views of the SMAQMD, their staff, employees, or contractors.

References

Anderson J.R., Hardy E.E., Roach J.T., Witmer R.E. (2001). *A land use and land cover classification system for use with remote sensor data. USGS Professional Paper 964.* Washington, DC: U.S. Government Printing Office.

Anthes, R. A. (1977). A cumulus parameterization scheme utilizing a one-dimensional cloud model. *Monthly Weather Review*, *105*, 270–286.

Akbari H., Rose S., Taha H. (1999). *Characterizing the fabric of the urban environment: A case study of Sacramento, California. Lawrence Berkeley National Laboratory report LBNL 44688.* Berkeley, California.

Betts, A. K., & Miller, M. J. (1986). A new convective adjustment scheme. Part II: Single column tests using GATE wave, BOMEX, and Arctic air-mass data sets. *Quarterly Journal of the Royal Meteorological Society*, *112*, 693–709.

Burian, S. J., Han, W. S., Velugubantla, S. P., & Maddula, S. R. K. (2003). *Development of gridded fields of urban canopy parameters for Models-3/CMAQ/MM5.* Salt Lake City, UT: Department of Civil and Environmental Engineering, University of Utah.

Campbell, G., & Norman, J. (1998). *An introduction to environmental biophysics* (2nd ed.). New York: Springer-Verlag.

Chen, F., & Dudhia, J. (2001). Coupling an advanced land surface/hydrology model with the Penn State/NCAR MM5 modeling system. Part I: Model implementation and sensitivity. *Monthly Weather Review*, *129*, 569–585.

Dudhia, J. (1993). A non-hydrostatic version of the Penn State/NCAR mesoscale model: Validation tests and simulation of an Atlantic cyclone and cold front. *Monthly Weather Review*, *121*, 1493–1513.

Duffie, J. A., & Beckman, W. A. (1980). *Solar engineering of thermal processes.* New York: John Wiley & Sons.

Dupont, S., Otte, T., & Ching, J. (2004). Simulation of meteorological fields within and above urban and rural canopies with a mesoscale model. *Boundary-Layer Meteorology*, *113*, 111–158.

Environ 2003. (2003). *Comprehensive air quality model with extensions version 4.* San Rafael, CA: Environ Corp., Air Sciences.

EPA (1991). *Guidelines for regulatory application of the Urban Airshed Model. U.S. Environmental Protection Agency Report EPA-450/4-91-013.* Office of Air Quality Planning and Standards, RTP, NC 27711.

EPA (1999). *Draft guidance on the use of models and other analyses in attainment demonstrations for the 8-hour ozone national ambient air quality standard.* EPA-454/R-99-004. EPA OAQPS, RTP, NC 27711.

Grell, G. A., Kuo, Y. H., & Pasch, R. (1991). Semi prognostic test of cumulus parameterization schemes in the middle latitudes. *Monthly Weather Review*, *119*, 5–31.

Grell G.A., Dudhia J., Stauffer D.R. (1994). *A description of the fifth generation PSU/NCAR mesoscale modeling system (MM5). Technical Note NCAR/TN—379+STR, NCAR.*

Guenther, A. B., Zimmerman, P. R., Harley, P. C., Monson, R. K., & Fall, R. (1993). Isoprene and monoterpene emission rate variability–model evaluations and sensitivity analyses. *Journal of Geophysical Research*, *98*, 12609–12617.

Hong, S. H., & Pan, H. L. (1996). Nonlocal boundary layer vertical diffusion in a medium-range forecast model. *Monthly Weather Review*, *124*, 2322–2339.

Hsie, E.-Y., & Anthes, R. A. (1984). Simulation of frontogenesis in a moist atmosphere using alternative parameterization of condensation and precipitation. *Journal of Atmospheric Sciences*, *41*, 2701–2716.

Kain, J. S., & Fritsch, J. M. (1993). Convective parameterization for mesoscale models: The Kain-Fritsch scheme. In K. A. Emanuel, & D. J. Raymond (Eds.), *The representation of cumulus convection in numerical models* (p. 246). Boston, MA: American Meteorological Society.

Martilli, A., Clappier, A., & Rotach, M. W. (2002). An urban surface exchange parameterization for mesoscale models. *Boundary-Layer Meteorology*, *104*, 261–304.

Masson, V. (2000). A physically-based scheme for the urban energy budget in atmospheric models. *Boundary-Layer Meteorology*, *94*, 357–397.

McPherson, E. G. (1998). Structure and sustainability of Sacramento's urban forest. *Journal of Arboriculture*, *24*, 174–190.

Mestayer P., Dupont S., Calmet I., Leroyer S., Mahuara A., Penelon T. (2004). *Soil Model for Sub-Meso scales – Urban (SM2-U). Model description document prepared for FUMAPEX (D4.4).* Nantes: ECN.

Pan, H. L., & Mahrt, L. (1987). Interaction between soil hydrology and boundary-layer development. *Boundary Layer Meteorology*, *38*, 185–202.

Reisner, J., Rasmussen, R. J., & Bruintjes, R. T. (1998). Explicit forecasting of supercooled liquid water in winter storms using the MM5 mesoscale model. *Quarterly Journal of the Royal Meteorological Society*, *124B*, 1071–1107.

Rose S., Akbari H., Taha H. (2003). *Characterizing the fabric of the urban environment: A case study of Greater Houston, Texas. Lawrence Berkeley National Laboratory report LBNL-51448*. Berkeley, California.

Salamanca, F., Martilli, A., Tewari, M., & Chen, F. (2011). A study of the urban boundary layer using different urban parameterizations and high-resolution urban canopy parameters with WRF. *Journal of Applied Meteorology and Climatology*, *50*, 1107–1128, http://dx.doi.org/10.1175/2010JAMC2538.1.

Schultz, P. (1995). An explicit cloud physics parameterization for operational numerical weather prediction. *Monthly Weather Review*, *123*, 3331–3343.

Seaman, N. L., Kain, J. S., & Deng, A. (1996). Development of a shallow convection parameterization for mesoscale models. In *Proceedings of the 11th AMS conference on numerical weather prediction* (pp. 340–342).

Simpson J., McPherson G. (2007). *Preliminary evaluation of the potential air quality benefits of trees within SIP guidelines.* Center for Urban Forest Research, PSW, USDA Forest Service (May 2007).

Skamarock W., Klemp J., Dudhia J., et al. (2008). *A description of the Advanced Research WRF. NCAR Technical Note NCAR/TN-475+STR.* Boulder, Colorado: National Center for Atmospheric Research.

Stauffer, D. R., & Seaman, N. L. (1990). Use of four-dimensional data assimilation in a limited-area mesoscale model. Part I: Experiments with synoptic-scale data. *Monthly Weather Review*, *118*, 1250–1277.

Taha, H. (1996). Modeling the impacts of increased urban vegetation on the ozone air quality in the south coast air basin. *Atmospheric Environment*, *30*, 3423–3430.

Taha H. (2005). *Surface modifications as a potential ozone air-quality improvement strategy in California: Part I: Mesoscale Modeling. Report prepared for the California Energy Commission, for Contract 500-02-013. Report 04-B, Altostratus Inc.* Available from the CEC website at: http://www.energy.ca.gov/2005publications/CEC-500-2005-128/CEC-500-2005-128.PDF.

Taha H. (2007). *Surface modifications as a potential ozone air-quality improvement strategy in California: Part II: Fine-resolution meteorological and photochemical modeling of urban heat islands. Report to the California Energy Commission, prepared by Altostratus Inc.* Available on the CEC web site at: http://www.energy.ca.gov/2009publications/CEC-500-2009-071/CEC-500-2009-071.PDF.

Taha, H. (2008a). Meso-urban meteorological and photochemical modeling of heat island mitigation. *Atmospheric Environment*, *42*, 8795–8809. http://dx.doi.org/10.1016/j.atmosenv.2008.06.036

Taha, H. (2008b). Episodic performance and sensitivity of the urbanized MM5 (uMM5) to perturbations in surface properties in Houston TX. *Boundary-Layer Meteorology*, *127*, 193–218. http://dx.doi.org/10.1007/s10546-007-9258-6

Taha, H. (2008c). Urban surface modification as a potential ozone air-quality improvement strategy in California: A mesoscale modeling study. *Boundary-Layer Meteorology*, *127*, 219–239. http://dx.doi.org/10.1007/s10546-007-9259-5

Taha H. (2011). *Multi-episodic and seasonal meteorological, air-quality, and emission-equivalence impacts of heat island control and evaluation of the potential atmospheric effects of urban solar photovoltaic arrays. Final report prepared by Altostratus Inc. for the California Energy Commission (CEC)*, PIER

Environmental Research Program, Sacramento, California. Report available at: http://www.energy.ca.gov/2013publications/CEC-500-2013-061/CEC-500-2013-061.pdf.

Taha H., Wilkinson J., Bornstein R. (2011). *Urban forest for clean air demonstration in the Sacramento Federal Noon-Attainment Area: Atmospheric modeling in support of a voluntary control measure. Final Report, prepared by Altostratus Inc. for the Sacramento Metropolitan Air Quality Management District, Sacramento, California.* Due to size, report can be obtained via FTP (ftp.altostratus.com, login: ftp2@altostratus.com, pass: ftpguest2).

Tao, W.-K., & Simpson, J. (1993). Goddard cumulus ensemble model. Part I: Model description. *Terrestrial, Atmospheric, and Oceanic Sciences*, *4*, 35–72.

Wesely, M. L. (1989). Parameterization of surface resistances to gaseous dry deposition in regional-scale numerical models. *Atmospheric Environment*, *23*, 1293–1304.

Xiao Q., Wu C. (2008). *Urban Forests for Clean Air Demonstration Project - Land Cover, Land Use, and Urban Forest Analysis. Report I: Analysis and Mapping of Current Land Use. Project report submitted to: Sacramento Tree Foundation*. Department of Land Air and Water Resources, University of California Davis.

Xiao Q., Wu C., Simpson J.R., McPherson E.G. (2009). *Urban Forests for Clean Air Demonstration Project - Land Cover, Land Use, and Urban Forest Analysis - Data collection, analysis and mapping of current land cover classification and urban forest structure.* Department of Land Air and Water Resources, University of California Davis and Center for Urban Forest Research, US Forest Service.

Yarwood, G., Morris, R. E., Yocke, M. A., Hogo, H., & Chico, T. (1996). Development of a methodology for source apportionment of ozone concentration estimates from a photochemical grid model. In *Proceedings of the 89th AWMA Annual Meeting*.